J. Geomag. Geoelectr., **49**, 1415–1437, 1997

Migration versus Inversion in Electromagnetic Imaging Technique

Michael S. ZHDANOV and Peter TRAYNIN

Department of Geology and Geophysics, University of Utah, Salt Lake City, UT 84112, U.S.A.

(Received January 31, 1997; Revised August 29, 1997; Accepted September 12, 1997)

One of the most challenging problems in electromagnetic (EM) geophysical methods is developing fast and stable methods of imaging inhomogeneous underground structures using EM data. In our previous publications we developed a novel approach to this problem, using EM migration.

In this paper we demonstrate that there is a very close connection between the method of EM migration and the solution of the conventional EM inverse problem. Actually, we show that migration is an approximate inversion. It realizes the first iteration in the inversion algorithm, based on the minimization of the residual field energy flow through the profile of observations. This new theoretical result opens a way for formulating a new imaging condition. We compare this new imaging condition with the traditional one, obtained for simplified geoelectrical models of the subsurface structures.

This result also leads to the construction of a solution of the inverse EM problem, based on iterative EM migration in the frequency domain, and gradient (or conjugate gradient) search for the optimal geoelectrical model. However, the authors have found that in the framework of this method, even the first iteration, based on the migration of the residual field, generates a reasonable geoelectrical image of the subsurface structure.

1. Introduction

One of the most challenging problems in electromagnetic (EM) geophysical methods is developing fast and stable methods of imaging inhomogeneous underground structures using EM data. Solution of this problem is important for many practical applications ranging from mineral exploration to waste and building site characterization. In the papers (Zhdanov *et al.*, 1995) and (Zhdanov *et al.*, 1996) and the references therein we have developed a novel approach to EM imaging based on the notion of EM migration. The method includes downward continuation of the observed field or one of its components in reverse time and application of the corresponding imaging conditions. However, until recently the relationship between EM migration imaging and traditional EM inversion have remained unexplored. The conventional EM inversion means a method which predicts the geoelectrical model generating the theoretical data closed to observations. The EM migration introduced in our previous publications constructed an image of subsurface geoelectrical structures, and there was no guarantee this image, if included in a geoelectrical model, would give rise to theoretical EM fields that matched those observed.

Meanwhile, Tarantola (1987) demonstrated that seismic wave migration, which was the prototype for EM migration, can be treated exactly as the first iteration in some general wave inversion scheme. In this paper we formulate an important new result: *EM migration, as the solution of the boundary value problem for the adjoint Maxwell's equation in frequency domain, can be clearly associated with the inverse problem solution.* In other words, we prove that a geoelectrical model constructed on the basis of migration images would actually generate a theoretical field close to observations.

We introduce the residual EM field as the difference between the simulated EM field for some given (background) geoelectrical model and the actual EM field. The EM energy flow of the residual field through the surface of observations can be treated as a functional of the anomalous conductivity distribution in the model. The analysis shows that the gradient of the residual field energy flow functional with respect to the perturbation of the model conductivity is equal to the integral over frequencies of the product of the incident (background) field and the migrated residual field, calculated as the solution of the boundary value problem for the adjoint Maxwell's equation.

This result clearly leads to a construction of the rigorous method of solving the inverse EM problem, based on iterative EM migration in the frequency domain, and gradient (or conjugate gradient) search for the optimal geoelectrical model. However, the authors have found that in the framework of this method, even the first iteration, based on the migration of the residual field, generates a reasonable geoelectrical image of the subsurface structure. We call the anomalous conductivity, calculated on the first iteration, *the migration apparent conductivity*. This new theoretical result suggests a new imaging condition formulation and indicates a new approach to EM imaging, based on iterative migration. The iterative migration forms a principally new method of interpreting EM data, which combines the ideas of downward continuation and traditional inversion. We compare this new imaging technique with the popular Rapid Relaxation Inversion (RRI) method developed by Smith and Booker (1991). Numerical modeling demonstrates that migration generates reasonable images of the subsurface structures even faster than rapid inversion.

In summary, in this paper we demonstrate that EM migration imaging can also be considered as the initial step in the general EM inversion procedure. This similarity facilitates better understanding the mathematical and physical background of EM migration, and, at the same time, develops new geoelectrical imaging tools.

For the sake of simplicity, in this paper we consider only the 2-D frequency domain geoelectrical problem. However, all the results, developed below can be generalized to the 3-D case. The solution of the 3-D migration and inversion problem is the subject of a separate paper, submitted to Geophysical Journal International (Zhdanov and Portniaguine, 1997).

2. 2-D EM Inverse Problem in the Frequency Domain

Consider a 2-D geoelectrical model with a background electrical conductivity $\sigma = \sigma_b$ and a local inhomogeneity D with conductivity $\sigma = \sigma_b + \Delta\sigma$, varying spatially. Note that the background conductivity in general case also can be a function of coordinate $\sigma_b = \sigma_b(x, z)$. However, it is assumed that it is known a priori. We assume that $\mu = \mu_0 = 4\pi \times 10^{-7}$H/m, where μ_0 is the free-space magnetic permeability. The model is excited by an E-polarized field generated by a linear current density $\mathbf{j}^{ex} = j^{ex}\mathbf{d}_y$, which is distributed in a domain Q in the upper half-plane ($z \leq 0$) with the constant conductivity $\sigma_b(x, z \leq 0) = \text{const}$. Here $\{\mathbf{d}_x, \mathbf{d}_y, \mathbf{d}_z\}$ is the orthonormal basis of the Cartesian system of coordinate with the origin on the earth's surface. This field is time harmonic as $e^{-i\omega t}$. We also consider the quasi-stationary model of the EM field, so displacement currents are neglected (Zhdanov and Keller, 1994). Within this model, the EM field can be described by a single function E_y satisfying the equation:

$$\begin{aligned} \nabla^2 E_y + i\omega\mu_0\sigma_b E_y &= -i\omega\mu_0 j^{ex}, \quad z \leq 0, \\ \nabla^2 E_y + i\omega\mu_0\sigma E_y &= 0, \quad z \geq 0, \end{aligned} \tag{1}$$

and the magnetic field components can be expressed by the equations:

$$H_x = -\frac{1}{i\omega\mu_0}\frac{\partial E_y}{\partial z}, \quad H_z = \frac{1}{i\omega\mu_0}\frac{\partial E_y}{\partial x}. \tag{2}$$

We can introduce the complex Poynting vector $\mathbf{P}$ as following (Stratton, 1941):

$$\mathbf{P} = \frac{1}{2}\mathbf{E} \times \mathbf{H}^* = \frac{1}{2}E_y H_z^* \mathbf{d}_x - \frac{1}{2}E_y H_x^* \mathbf{d}_z, \tag{3}$$

where in the case of E-polarization $\mathbf{E} = E_y \mathbf{d}_y$, $\mathbf{H}^* = H_x^* \mathbf{d}_x + H_z^* \mathbf{d}_z$ and $*$ indicates a complex conjugate value. The real part of the vector $\mathbf{P}$ describes the intensity of the EM field energy flow. The divergence of the real part of $\mathbf{P}$ determines the energy dissipated in heat per unit volume per second:

$$\nabla \cdot Re\mathbf{P} = -\frac{1}{2}\sigma \mathbf{E} \cdot \mathbf{E}^*. \tag{4}$$

It can be shown using 2D Green's theorem that the total energy Q dissipated throughout any region S bounded by a contour L is equal to:

$$Q = -Re \int_L \mathbf{P} \cdot \mathbf{n} dl = \frac{1}{2} \iint_S \sigma \mathbf{E} \cdot \mathbf{E}^* ds \geq 0, \tag{5}$$

where $\mathbf{n}$ is the unit outward normal vector and the contour is traversed counterclockwise.

When the region S coincides with the lower half-plane ($z \geq 0$), the contour L can be composed of the horizontal axis $z = 0$ and an infinitely large semicircle in the lower half-plane. Since the EM field satisfies to the radiation conditions, i.e., functions $\mathbf{E}$ and $\mathbf{H}^*$ vanish exponentially at infinity , the contour integral over infinitely large semicircle tends to zero. Thus, the total energy Q dissipated in the lower half-plane can be calculated using the formula:

$$Q = Re \int_{-\infty}^{+\infty} \mathbf{P} \cdot \mathbf{d}_z dl = -\frac{1}{4} \int_{-\infty}^{+\infty} \left(E_y H_x^* + E_y^* H_x \right) dx', \tag{6}$$

where x' is the integration variable and we use the formula $Re\left(E_y H_x^*\right) = \frac{1}{2}\left(E_y H_x^* + E_y^* H_x\right)$.

Let us denote the EM field components observed on the surface of the Earth ($z = 0$) at the point x' as $E_y^{obs}(x', o, \omega)$, $H_x^{obs}(x', o, \omega)$ and also denote the theoretical EM field components calculated for a given background geoelectrical model $\sigma_b(x, z)$ as $E_y^b(x', o, \omega)$, $H_x^b(x', o, \omega)$. We can introduce the residual fields as the difference between the observed and background theoretical fields:

$$\begin{aligned} E_y^\Delta(x', o, \omega) &= E_y^{obs}(x', o, \omega) - E_y^b(x', o, \omega), \\ H_x^\Delta(x', o, \omega) &= H_x^{obs}(x', o, \omega) - H_x^b(x', o, \omega). \end{aligned} \tag{7}$$

The observed field is generated by the real geoelectrical cross section $\sigma(x, z) = \sigma_b(x, z) + \Delta\sigma(x, z)$ and actually exists everywhere in the vertical section. Therefore, the residual field can be determined everywhere as a function of coordinates (x, z) and satisfies the equations:

$$\begin{aligned} &\nabla^2 E_y^\Delta + i\omega\mu_0\sigma_b E_y^\Delta = 0, \quad z \leq 0, \\ &\nabla^2 E_y^\Delta + i\omega\mu_0\sigma_b E_y^\Delta = -i\omega\mu_0\Delta\sigma E_y^{obs}, \quad z \geq 0, \\ &H_x^\Delta = -\frac{1}{i\omega\mu_0}\frac{\partial E_y^\Delta}{\partial z}, \quad H_z^\Delta = \frac{1}{i\omega\mu_0}\frac{\partial E_y^\Delta}{\partial x}. \end{aligned} \tag{8}$$

The total energy flow Q^Δ of the residual field through the earth's surface ($z = 0$), is calculated by the formula:

$$Q^\Delta = -Re \int_{-\infty}^{+\infty} \mathbf{P}^\Delta \cdot \mathbf{d}_z dl = \frac{1}{4} \int_{-\infty}^{+\infty} \left(E_y^\Delta H_x^{\Delta*} + E_y^{\Delta*} H_x^\Delta \right) dx', \tag{9}$$

where we use the "+" sign, opposite to the sign of the expression (6), because the sources of the residual field, excess currents in the inhomogeneity D, are located in the lower half-plane. Pankratov, Avdeev and Kuvshinov (1995) have proved an important theorem, according to which the energy flow Q^{Δ} of the residual field is non-negative:

$$Q^{\Delta} \geq 0. \tag{10}$$

Moreover, if the conductivity of the upper half-plane is assumed to be nonzero ($\sigma_b > 0$) the residual field energy flow is always positive (for residual field not identically equal to zero $E_y^{\Delta} \neq 0$). This result can be obtained from the Eq. (5) applied to the upper half-plane:

$$Q^{\Delta} = \frac{\sigma_b}{2} \iint_{z \leq 0} E_y^{\Delta} E_y^{\Delta *} ds = \frac{\sigma_b}{2} \iint_{z \leq 0} \left| E_y^{\Delta} \right|^2 ds > 0,\ if\ E_y^{\Delta} \neq 0. \tag{11}$$

Based on this theorem we can introduce the measure Φ of the difference between the observed and the background theoretical fields as the residual field energy flow, integrated over the frequency range Ω:

$$\Phi(\sigma_b) = \int_{\Omega} Q^{\Delta} d\omega = \frac{1}{4} \int_{\Omega} \int_{-\infty}^{+\infty} \left(E_y^{\Delta} H_x^{\Delta *} + E_y^{\Delta *} H_x^{\Delta} \right) dx' d\omega. \tag{12}$$

The functional $\Phi(\sigma_b)$ can be treated as an analog of the misfit between the observed and theoretical fields. The advantage of this new functional in comparison with the traditional misfit functional is that $\Phi(\sigma_b)$ has a clear physical meaning of the residual field energy flow through the profile of observations.

Obviously, the background theoretical field components $E_y^b(x', o, \omega)$ and $H_x^b(x', o, \omega)$ depend on the conductivity distribution $\sigma_b(x,z)$ in the given geoelectrical model and, therefore, Φ can be treated as a functional of the conductivity model: $\Phi = \Phi(\sigma_b)$. We would like to modify the background conductivity in such a way that it will be equal to the actual conductivity within the anomalous domain D. In this case the new background field will be close to the observed field.

Thus, the 2-D EM inversion problem can be reduced to the minimization of the functional:

$$\Phi(\sigma_b) = \min. \tag{13}$$

In the following section we will discuss an approach to the solution of this problem.

Note that the analysis given in this section for the TE mode applies in an analogues manner to the TM mode. It is important to notice also that similar to the case of the traditional misfit functional it is possible to incorporate measurement uncertainties in the functional Φ given by Eq. (12) by using weighted data. In this case this functional will correspond to the energy of the weighted EM data.

3. The Steepest Descent Method of Nonlinear Inversion

We begin our analysis with the formulation of the steepest descent method of solving the minimization problem (13). The critical problem in realizing any steepest descent method is the calculation of the steepest ascent direction (or the gradient) of the functional. To solve this problem, let us perturb the background conductivity distribution: $\sigma_b'(x,z) = \sigma_b(x,z) + \delta\sigma(x,z)$. Actually, we have to perturb the conductivity only within the inhomogeneous domain D of the lower half-plane:

$$\delta\sigma(x,z) = 0, \quad (x,z) \notin D. \tag{14}$$

The first variation of the misfit functional with respect to the perturbation of the background conductivity can be calculated as:

$$\delta\Phi(\sigma, \delta\sigma) = \frac{1}{4} \int_{\Omega} \int_{-\infty}^{+\infty} \left(\delta E_y^{\Delta} H_x^{\Delta *} + E_y^{\Delta} \delta H_x^{\Delta *} + \delta E_y^{\Delta *} H_x^{\Delta} + E_y^{\Delta *} \delta H_x^{\Delta} \right) dx' d\omega. \tag{15}$$

where we use the "+" sign, opposite to the sign of the expression (6), because the sources of the residual field, excess currents in the inhomogeneity D, are located in the lower half-plane. Pankratov, Avdeev and Kuvshinov (1995) have proved an important theorem, according to which the energy flow Q^{Δ} of the residual field is non-negative:

$$Q^{\Delta} \geq 0. \tag{10}$$

Moreover, if the conductivity of the upper half-plane is assumed to be nonzero ($\sigma_b > 0$) the residual field energy flow is always positive (for residual field not identically equal to zero $E_y^{\Delta} \neq 0$). This result can be obtained from the Eq. (5) applied to the upper half-plane:

$$Q^{\Delta} = \frac{\sigma_b}{2} \iint_{z \leq 0} E_y^{\Delta} E_y^{\Delta *} ds = \frac{\sigma_b}{2} \iint_{z \leq 0} \left| E_y^{\Delta} \right|^2 ds > 0, \; if \; E_y^{\Delta} \neq 0. \tag{11}$$

Based on this theorem we can introduce the measure Φ of the difference between the observed and the background theoretical fields as the residual field energy flow, integrated over the frequency range Ω:

$$\Phi(\sigma_b) = \int_{\Omega} Q^{\Delta} d\omega = \frac{1}{4} \int_{\Omega} \int_{-\infty}^{+\infty} \left(E_y^{\Delta} H_x^{\Delta *} + E_y^{\Delta *} H_x^{\Delta} \right) dx' d\omega. \tag{12}$$

The functional $\Phi(\sigma_b)$ can be treated as an analog of the misfit between the observed and theoretical fields. The advantage of this new functional in comparison with the traditional misfit functional is that $\Phi(\sigma_b)$ has a clear physical meaning of the residual field energy flow through the profile of observations.

Obviously, the background theoretical field components $E_y^b(x', o, \omega)$ and $H_x^b(x', o, \omega)$ depend on the conductivity distribution $\sigma_b(x, z)$ in the given geoelectrical model and, therefore, Φ can be treated as a functional of the conductivity model: $\Phi = \Phi(\sigma_b)$. We would like to modify the background conductivity in such a way that it will be equal to the actual conductivity within the anomalous domain D. In this case the new background field will be close to the observed field.

Thus, the 2-D EM inversion problem can be reduced to the minimization of the functional:

$$\Phi(\sigma_b) = \min. \tag{13}$$

In the following section we will discuss an approach to the solution of this problem.

Note that the analysis given in this section for the TE mode applies in an analogues manner to the TM mode. It is important to notice also that similar to the case of the traditional misfit functional it is possible to incorporate measurement uncertainties in the functional Φ given by Eq. (12) by using weighted data. In this case this functional will correspond to the energy of the weighted EM data.

3. The Steepest Descent Method of Nonlinear Inversion

We begin our analysis with the formulation of the steepest descent method of solving the minimization problem (13). The critical problem in realizing any steepest descent method is the calculation of the steepest ascent direction (or the gradient) of the functional. To solve this problem, let us perturb the background conductivity distribution: $\sigma_b'(x, z) = \sigma_b(x, z) + \delta\sigma(x, z)$. Actually, we have to perturb the conductivity only within the inhomogeneous domain D of the lower half-plane:

$$\delta\sigma(x, z) = 0, \;\; (x, z) \notin D. \tag{14}$$

The first variation of the misfit functional with respect to the perturbation of the background conductivity can be calculated as:

$$\delta\Phi(\sigma, \delta\sigma) = \frac{1}{4} \int_{\Omega} \int_{-\infty}^{+\infty} \left(\delta E_y^{\Delta} H_x^{\Delta *} + E_y^{\Delta} \delta H_x^{\Delta *} + \delta E_y^{\Delta *} H_x^{\Delta} + E_y^{\Delta *} \delta H_x^{\Delta} \right) dx' d\omega. \tag{15}$$

Here δE_y^{Δ}, $\delta H_x^{\Delta *}$ are the first variations of the residual electric and magnetic fields:

$$\begin{aligned} \delta E_y^{\Delta} &= \delta\left(E_y^{obs}\left(x', o, \omega\right) - E_y^{b}\left(x', o, \omega\right)\right) = -\delta E_y^{b}\left(x', o, \omega\right), \\ \delta H_x^{\Delta *} &= \delta\left(H_x^{obs *}\left(x', o, \omega\right) - H_x^{b *}\left(x', o, \omega\right)\right) = -\delta H_x^{b *}\left(x', o, \omega\right), \end{aligned} \tag{16}$$

using $\delta E_y^{obs} = \delta H_x^{obs *} = 0$.

According to Appendix A the first variations of the background electric and magnetic fields can be calculated as:

$$\delta E_y^{b}\left(x', 0, \omega\right) = i\omega\mu_0 \iint_D G_{\sigma_b} \delta\sigma E_y^{b} ds, \tag{17}$$

$$\delta H_x^{b}\left(x', 0, \omega\right) = -\iint_D \frac{\partial G_{\sigma_b}}{\partial z'} \delta\sigma E_y^{b} ds, \tag{18}$$

where G_{σ_b} is the Green's function of the geoelectrical model with the background conductivity $\sigma_b = \sigma_b\left(x, z\right)$. Substituting Eqs. (17) and (18) into Eqs. (16) and (15) and changing the order of integration, we obtain:

$$\begin{aligned} \delta\Phi\left(\sigma, \delta\sigma\right) = -\frac{1}{4} \iint_D \delta\sigma \int_\Omega \int_{-\infty}^{+\infty} & \left(i\omega\mu_0 G_{\sigma_b} E_y^{b} H_x^{\Delta *} - E_y^{\Delta} \frac{\partial G_{\sigma_b}^{*}}{\partial z'} E_y^{b *} \right. \\ & \left. - i\omega\mu_0 G_{\sigma_b}^{*} E_y^{b *} H_x^{\Delta} - E_y^{\Delta *} \frac{\partial G_{\sigma_b}}{\partial z'} E_y^{b} \right) dx' d\omega ds. \end{aligned} \tag{19}$$

At the same time the residual magnetic field H_x^{Δ} can be expressed as the vertical derivative of the residual electric field E_y^{Δ} using the equation:

$$H_x^{\Delta} = -\frac{1}{i\omega\mu_0} \frac{\partial E_y^{\Delta}}{\partial z'}. \tag{20}$$

Taking the last equation into account we can modify Eq. (19):

$$\begin{aligned} \delta\Phi\left(\sigma, \delta\sigma\right) &= -\frac{1}{4} \iint_D \delta\sigma \int_\Omega E_y^{b} \cdot \int_{-\infty}^{+\infty} \left(G_{\sigma_b} \frac{\partial E_y^{*\Delta}}{\partial z'} - E_y^{\Delta *} \frac{\partial G_{\sigma_b}}{\partial z'} \right) dx' d\omega ds \\ &= -\frac{1}{4} \iint_D \delta\sigma \int_\Omega E_y^{b *} \cdot \int_{-\infty}^{+\infty} \left(G_{\sigma_b}^{*} \frac{\partial E_y^{\Delta}}{\partial z'} - E_y^{\Delta} \frac{\partial G_{\sigma_b}^{*}}{\partial z'} \right) dx' d\omega ds. \end{aligned} \tag{21}$$

According to Appendix B:

$$\int_{-\infty}^{+\infty} \left(G_{\sigma_b}^{*} \frac{\partial E_y^{\Delta}}{\partial z'} - E_y^{\Delta} \frac{\partial G_{\sigma_b}^{*}}{\partial z'} \right) dx' = E_y^{\Delta m *}, \tag{22}$$

and

$$\int_{-\infty}^{+\infty} \left(G_{\sigma} \frac{\partial E_y^{*\Delta}}{\partial z'} - E_y^{\Delta *} \frac{\partial G_{\sigma}}{\partial z'} \right) dx' = E_y^{\Delta m}, \tag{23}$$

where $E_y^{\Delta m}$ is the migrated residual electric field, determined in Appendix B.

Substituting Eqs. (22) and (23) back to Eq. (21) we obtain:

$$\begin{aligned} \delta\Phi\left(\sigma_b, \delta\sigma\right) &= -\frac{1}{4} \iint_S \delta\sigma \int_\Omega \left(E_y^{b} E_y^{\Delta m} + E_y^{b *} E_y^{\Delta m *} \right) d\omega ds \\ &= -\frac{1}{2} \iint_S \delta\sigma Re \int_\Omega E_y^{b} E_y^{\Delta m} d\omega ds. \end{aligned} \tag{24}$$

Therefore, to make the first variation of the misfit functional to be negative we have to select $\delta\sigma$ as:

$$\delta\sigma(x,z) = -k_0 l(x,z), \ (x,z) \in D, \tag{25}$$

where the gradient direction $l(x,z)$ (or direction of the steepest ascent) is computed using the expression:

$$l(x,z) = -Re \int_\Omega E_y^b E_y^{\Delta m} d\omega, \tag{26}$$

and k_0 is a positive number (length of a step). This choice of $\delta\sigma$ makes

$$\delta\Phi(\sigma_b, \delta\sigma) = -\frac{1}{2} k_0 \iint_S \left[Re \int_\Omega E_y^b E_y^{\Delta m} d\omega \right]^2 ds,$$

which is indeed negative.

Thus, we can see that *the gradient direction of the residual field energy flow functional is equal to the integral over frequencies of the product of the incident (background) field and the migrated residual field.*

Let us select the initial conductivity distribution model to be equal to the background conductivity:

$$\sigma_{(0)}(x,z) = \sigma_b(x,z). \tag{27}$$

The first iteration of the conductivity can be found as:

$$\sigma_{(1)}(x,z) = \sigma_{(0)}(x,z) + \delta\sigma(x,z) = \sigma_b(x,z) - k_0 l(x,z), \ (x,z) \in D. \tag{28}$$

Formula (28) describes the first approximation to the conductivity distribution. We can see from Eqs. (25) and (26) that the anomalous conductivity $\delta\sigma(x,z)$ is proportional (with some constant coefficient k_0) to the frequency stacked values of the product of the background (incident) field E_y^b (the field that corresponds to the background distribution of conductivity $\sigma_{(0)}(x,z) = \sigma_b(x,z)$) and the migrated residual field $E_y^{\Delta m} = \left[E_y^{obs}(x', o, \omega) - E_y^b(x', o, \omega)\right]^m$. In the time domain the stacking formula corresponds to the convolution of the background and migrated electric field (Zhdanov and Portniaguine, 1997).

The optimal length of the step k_0 can be determined by a linear search for the minimum of the functional:

$$\Phi[\sigma_b(x,z) - k_0 l(x,z)] = \Phi(k_0) = \min \tag{29}$$

with respect to k_0. Derivations presented in Appendix C show that k_0 can be determined by the formula:

$$k_0 = -\frac{Re \int_\Omega \int_{-\infty}^{+\infty} \left[E_y^l H_x^{\Delta *} + E_y^{\Delta} H_x^{l*}\right] dx' d\omega}{2Re \int_\Omega \int_{-\infty}^{+\infty} E_y^l H_x^{l*} dx' d\omega}, \tag{30}$$

where E_y^l is migration field, calculated for the model perturbed in the gradient direction.

Note in the conclusion of this section that we have discussed above the iterative migration method based on steepest descent method. It is well known that this method usually converges more slowly than Newton method or conjugate gradient (CG) method. However, using the expression for steepest ascent direction (26) one can easily apply the CG search for the optimal geoelectrical model. We don't present here the full description of CG migration due to the limited size of a journal paper. At the same time, we will demonstrate below that even migration based on the first iteration of the steepest descent method can produce reasonable geophysical results.

Thus, on the basis of Eqs. (25) and (26), we can introduce the migration apparent conductivity as:

$$\Delta\sigma_{ma}(x,z) = k_0 Re \int_\Omega E_y^b(x,z) E_y^{\Delta m}(x,z) d\omega. \tag{31}$$

4. Iterative Migration

We have demonstrated above that the conventional migration imaging introduced in our paper (Zhdanov and Keller, 1994) and others, can be treated as the first iteration in the solution of some specific EM inverse problem, formulated in Section 2. Obviously, we can obtain better imaging results if we repeat the iterations. The general iterative process can be described by the formulae:

$$\sigma_{(n+1)}(x,z) = \sigma_{(n)}(x,z) + \delta\sigma_{(n)}(x,z) = \sigma_{(n)}(x,z) - k_n l_n(x,z), \ (x,z) \in D. \tag{32}$$

The gradient direction on the n-th iteration $l_n(x,z)$ can be calculated by the formula, analogous to Eq. (26):

$$l_n(x,z) = -Re \int_\Omega E_y^n E_y^{\Delta_n m} d\omega, \tag{33}$$

where E_y^n is the field calculated by forward modeling for the geoelectrical model with the conductivity distribution $\sigma_{(n)}(x,z)$, and $E_y^{\Delta_n m}$ is the migrated residual field $E_y^{\Delta_n}$, computed as the difference between the observed field and the theoretical field E_y^n, found on the n-th iteration:

$$\begin{aligned} E_y^{\Delta_n}(x',o,\omega) &= E_y^{obs}(x',o,\omega) - E_y^n(x',o,\omega), \\ H_x^{\Delta_n}(x',o,\omega) &= H_x^{obs}(x',o,\omega) - H_x^n(x',o,\omega). \end{aligned} \tag{34}$$

The optimal length of the step k_n can be determined by the formula, similar to (30):

$$k_n = -\frac{Re \int_\Omega \int_{-\infty}^{+\infty} \left[E_y^{l_n} H_x^{\Delta_n *} + E_y^{\Delta_n} H_x^{l_n *}\right] dx' d\omega}{2Re \int_\Omega \int_{-\infty}^{+\infty} E_y^{l_n} H_x^{l_n *} dx' d\omega,} \tag{35}$$

where $E_y^{l_n}$ is the electric field, calculated for the model $\sigma_{(n)}(x,z)$, perturbed in the gradient direction.

Note that the iteration scheme described above does not include regularization, so the solution can be unstable. To obtain a regularized solution we should introduce a Tikhonov parametric functional:

$$P^\alpha(\sigma) = \Phi(\sigma) + \alpha S(\sigma), \tag{36}$$

where α is a regularization parameter, and $S(\sigma)$ is a stabilizer that can be determined as an L_2 norm of the difference between the current conductivity distribution σ and some a priori model of the conductivity σ_{apr}

$$S(\sigma) = \|\sigma - \sigma_{apr}\|_{L_2}^2 = \iint_D [\sigma(x,z) - \sigma_{apr}(x,z)]^2 ds. \tag{37}$$

The a priori model is usually selected based on available geological and geophysical information.

In this case the iterative process is described by the formula:

$$\sigma_{(n+1)}(x,z) = \sigma_{(n)}(x,z) - k_n^{(\alpha)} l_n^{(\alpha)}(x,z), \tag{38}$$

where $l_n^{(\alpha)}(x,z)$ is the regularized gradient direction on the n-th iteration, calculated by the formula:

$$l_n^{(\alpha)}(x,z) = -Re \int_\Omega E_y^n E_y^{\Delta_n m} d\omega + \alpha(\sigma_n - \sigma_{apr}), \tag{39}$$

and the length of the regularized step $k_n^{(\alpha)}$ is calculated using the linear search for the minimum of the parametric functional:

$$P^{\alpha}\left(\sigma_{(n)} - k_n^{(\alpha)} l_n^{(\alpha)}\right) = \mathbf{P}^{\alpha}\left(k_n^{(\alpha)}\right) = \min . \tag{40}$$

Thus, we can describe the developed method of EM inversion as the process of iterative migration. On every iteration we calculate the theoretical EM response for the given geoelectrical model $\sigma_{(n)}(x, z)$, obtained on the previous step, calculate the residual field between this response and the observed field, and then migrate the residual field. The gradient direction is computed as the stack over the frequencies of the product of the migrated residual field and the theoretical response E_y^n. Using this gradient direction and the corresponding value of the optimal length of the step $k_n^{(\alpha)}$, we calculate the new geoelectrical model $\sigma_{(n+1)}(x, z)$ on the basis of expression (38). The iterations are terminated when the functional $\Phi(\sigma)$ reaches the level of the noise energy. The optimal value of the regularization parameter α is selected using conventional principles of regularization theory, described, for example, in Zhdanov and Keller (1994) or Zhdanov (1993).

5. Numerical Models

We analyze the properties of new imaging conditions, introduced in this paper, on simple synthetic models. We have calculated the theoretical EM fields for these models using the code PW2D discussed by Wannamaker *et al.* (1987). For numerical calculation of the migration field we use finite-difference code, developed in our paper (Zhdanov *et al.*, 1996).

Figure 1(a) depicts a locally conductive rectangular-insert 2-D model. The resistivity of the inclusion is 0.5 Ohm-m and the resistivity of the host rocks is 250 Ohm-m. The synthetic "observed field" components were calculated using the same PW2D forward modeling code. The $N = 61$ observation points x_i ($i = 1, 2, \ldots, N$) were located along the profile on the earth's surface with the separation $\Delta x = 1000$ m. We have computed the electric E_y and magnetic H_x fields for the $J = 42$ periods within the range 0.01–0.25 sec. The result of migration imaging for multifrequency TE mode EM data is shown in Fig. 1(b),(c),(d) (1st, 2nd and 4th iterations). One can see that even migration image obtained on the 1st iteration reconstructs well the location of the inhomogeneity. However, the conductivity contrast is underestimated. The 4th iteration reproduces well both the geometry and the conductivity of the rectangular body. Figure 2 presents the plots of the normalized residual energy functional $\widetilde{\Phi}$ computed by discrete analog of formula (12) and the traditional normalized least square misfit functional φ_ρ computed for apparent resistivity differencies for all 4 iterations:

$$\widetilde{\Phi} = \frac{\sum_{i=1}^{N}\sum_{j=1}^{J}\left[E_y^{\Delta}(x_i,\omega_j)\,H_x^{\Delta *}(x_i,\omega_j) + E_y^{\Delta *}(x_i,\omega_j)\,H_x^{\Delta}(x_i,\omega_j)\right]}{\sum_{i=1}^{N}\sum_{j=1}^{J}\left[E_y^{obs}(x_i,\omega_j)\,H_x^{obs*}(x_i,\omega_j) + E_y^{obs*}(x_i,\omega_j)\,H_x^{obs}(x_i,\omega_j)\right]},$$

$$\varphi_\rho = \frac{\sum_{i=1}^{N}\sum_{j=1}^{J}\left|\rho_a^{obs}(x_i,\omega_j) - \rho_a^{(n)}(x_i,\omega_j)\right|^2}{\sum_{i=1}^{N}\sum_{j=1}^{J}\left|\rho_a^{obs}(x_i,\omega_j)\right|^2},$$

where ρ_a^{obs} is observed magnetotelluric resistivity and $\rho_a^{(n)}$ is theoretical predicted apparent resistivity computed by the formulae:

$$\rho_a^{obs} = \frac{1}{\omega\mu_0}\left|\frac{E_y^{obs}}{H_x^{obs}}\right|, \quad \rho_a^{(n)} = \frac{1}{\omega\mu_0}\left|\frac{E_y^{n}}{H_x^{n}}\right|. \tag{41}$$

We can observe a fast convergence of the iterative migration on these plots. Note that CPU time for computing one migration iteration is approximately equal to 20 s on Spark 4 Work Station,

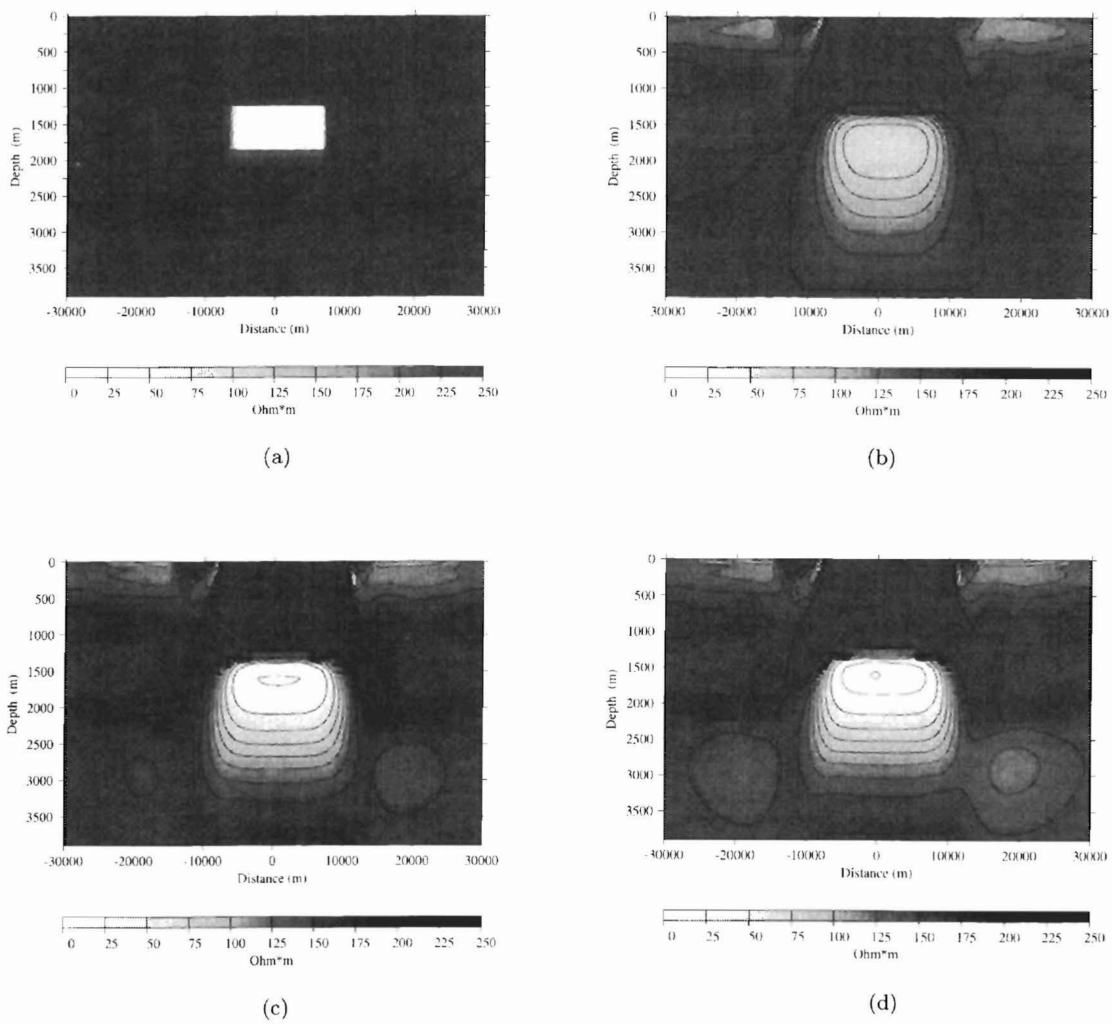

Fig. 1. (a) 2-D resistivity model of a locally conductive rectangular-insert. The resistivity of the inclusion is 0.5 Ohm-m and the resistivity of the host rocks is 250 Ohm-m; (b) The result of the 1st iteration migration imaging, stacked over the time periods range 0.01–0.25 s; (c) The result of the 2nd iteration migration imaging, stacked over the time periods range 0.01–0.25 s; (d) The result of the 4th iteration migration imaging, stacked over the time periods range 0.01–0.25 s.

which is 2–3 times faster than the forward modeling solution. So, the most time consuming part of the iterative migration is the forward modeling. For example, the total CPU time for computing the 4th iteration presented in Fig. 1 is approximately equal to 4 minutes.

Figure 3 shows the apparent resistivity curves computed at the point $x = 0$ m on the surface of the earth for geoelectrical models obtained by 1st, 2nd and 4th migration iterations. One can see that these plots converge to the observed apparent resistivity curve (shown by solid lines).

We compare the migration results with the inversion by the popular Rapid Relaxation Inversion (RRI) technique developed by Smith and Booker (1991). Figure 4 presents the RRI image

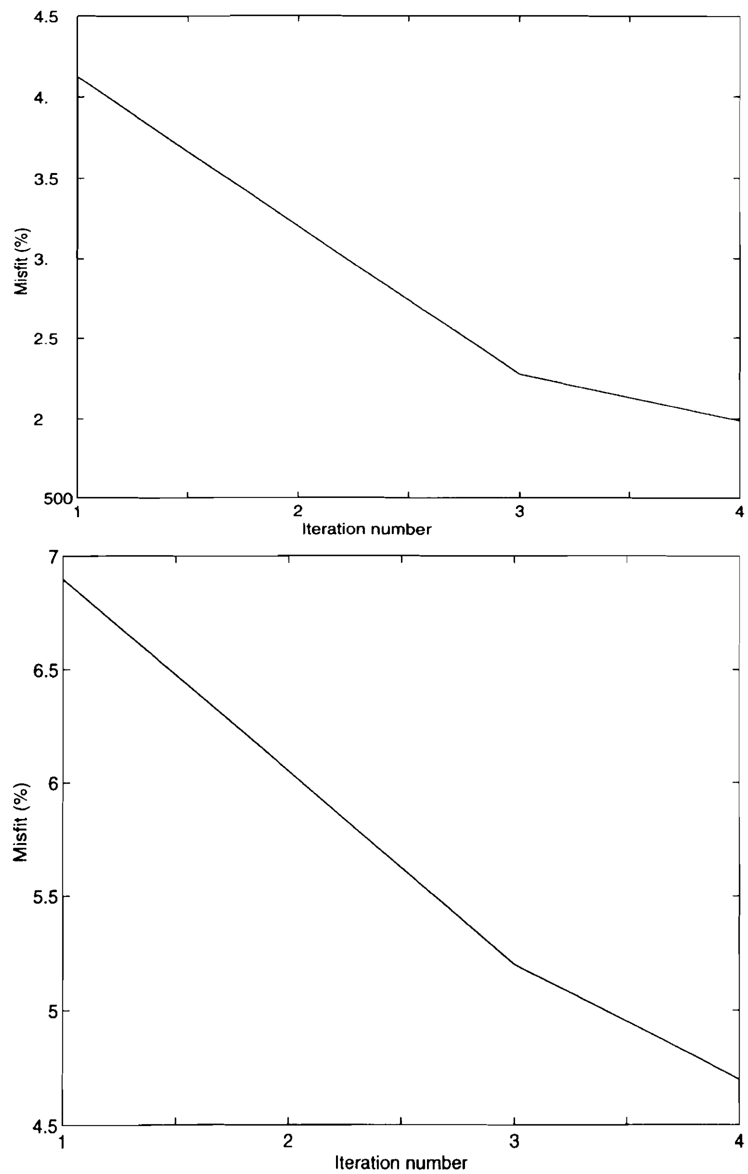

Fig. 2. The plots of the normalized residual energy functional $\widetilde{\Phi}$ computed by discrete analog of formula (12) and the traditional normalized least square misfit functional φ_ρ computed for apparent resistivity differencies for the model shown in Fig. 1(a).

obtained for the same model shown in Fig. 1(a). It took 30 iterations and about 30 Min of CPU time to generate this model. The misfit between the synthetic observed data and the theoretical field generated by RRI for the model presented in Fig. 4 is equal to 1.54%. One can see that in spite of the small value of the misfit, the model obtained by RRI describes the real rectangular insert not as clearly as the migration image. The RRI produces a more diffuse and unfocused image of the real geoelectrical structure than even the 1st iteration migration.

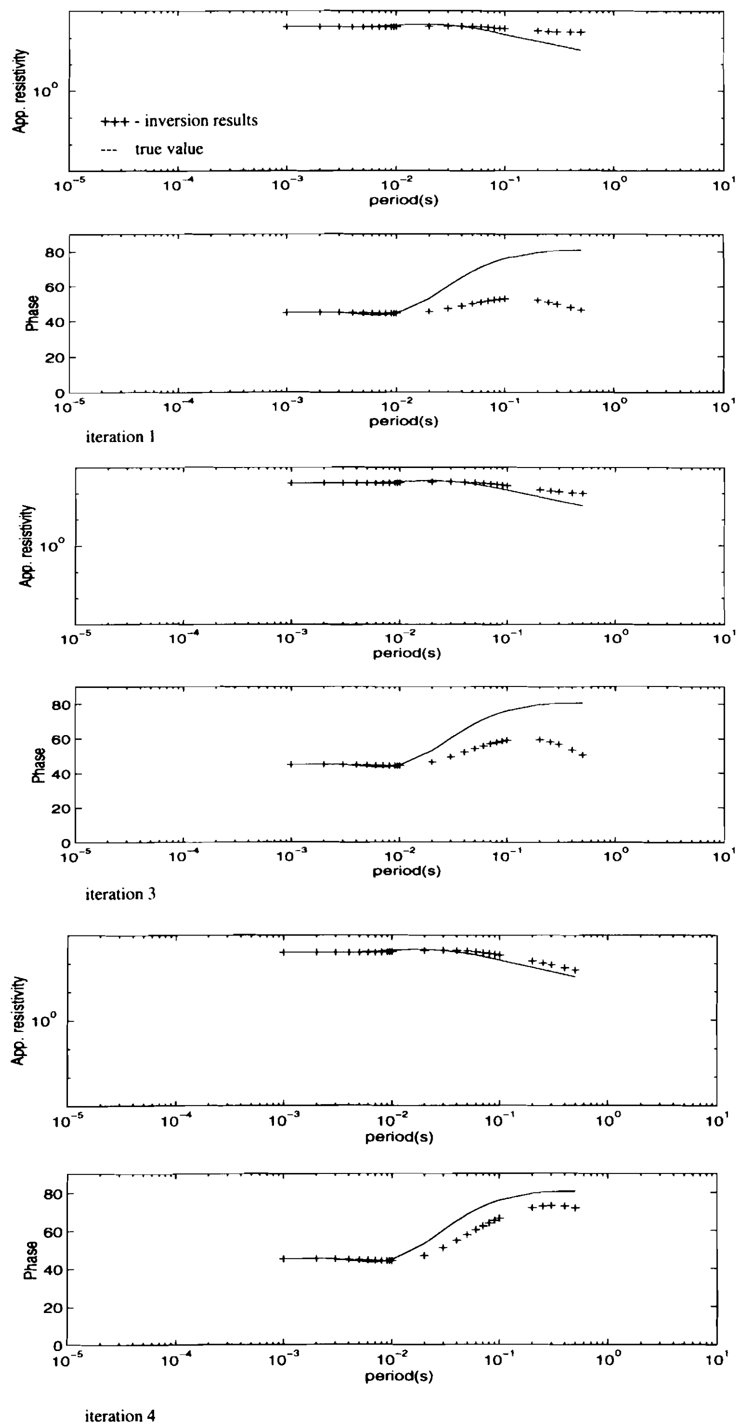

Fig. 3. The apparent resistivity curves and phases computed at the point $x = 0$ m on the surface of the earth for geoelectrical models obtained by 1st, 2nd and 4th migration iterations for the model shown in Fig. 1(a) (dash lines). The observed apparent resistivity and phase curves are shown by solid lines.

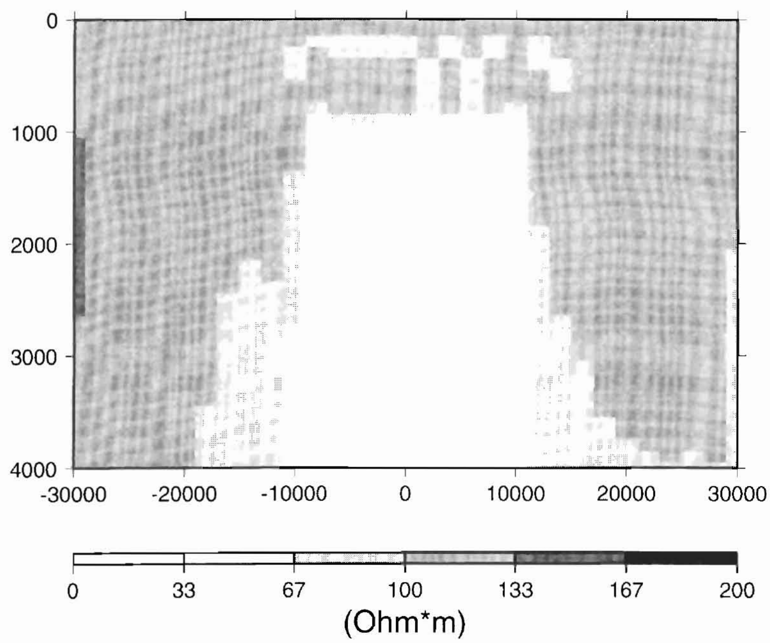

Fig. 4. The inverse model obtained for the model shown in Fig. 1(a) using Rapid Relaxation Inversion (RRI) code by Booker and Smith (1991) after 30 iterations.

Figure 5 presents a 2-D model of a prismatic conductive prism with the horizontal shear strain applied. Conductivity parameters of the model are the same as in the previous example. We also use the same observation points and frequency for observed TE mode EM field. The result of the 1st iteration migration is shown in Fig. 6. The image reflects the direction of the deformation. It takes only 20 s of CPU time to generate this image. At the same time RRI produces the inverse model presented in Fig. 7 after 35 iterations, and it requires 32 Min on Sparc-4 Work Station. The RRI model itself doesn't describe better the geometry of the real conductive body than the migration image. However, 1st iteration migration underestimates the conductivity contrast while RRI produces a correct estimation. To obtain the correct anomalous conductivity by migration we have to run the migration iteratively several times, as it has been demonstrated above for the model in Fig. 1. Meanwhile, if we would like to get a quick image of the subsurface structures without paying much attention to exact conductivity contrasts, the 1st iteration migration can solve this problem quite reasonably.

Note that the migration images for examples described above were computed for different individual frequencies, and stacked over the range of frequencies. Stacking for a spectrum of frequencies results in positive reinforcement within the inhomogeneity and destructive interference elsewhere.

However, even images for individual frequencies possess the necessary resolution, as we can see for the next model of two conductive rectangular inserts with resistivities 0.5 Ohm-m within a 250 Ohm-m background, presented in Fig. 8. Figure 9 shows the migration image computed for the period 0.05 s. For comparison we have applied the RRI to the same data and have obtained a geoelectrical model presented in Fig. 10. This model, similar to one shown in Fig. 4, gives a rather diffusive image of actual structures. However, misfit between the observed and theoretical data for this model is very small and equal 1.54%. The CPU time for migration is 22 s, while the

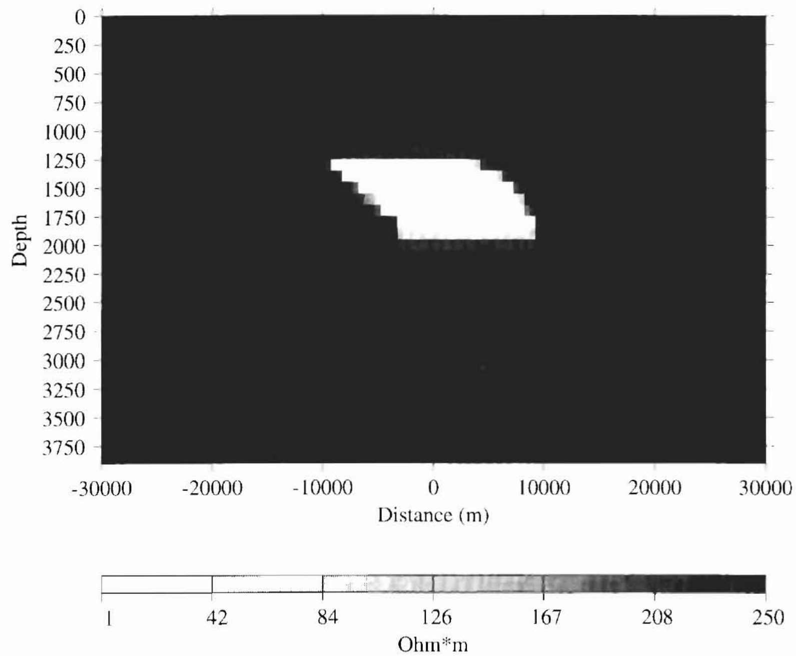

Fig. 5. 2-D resistivity model of a prismatic conductive insert with the horizontal shear strain applied.

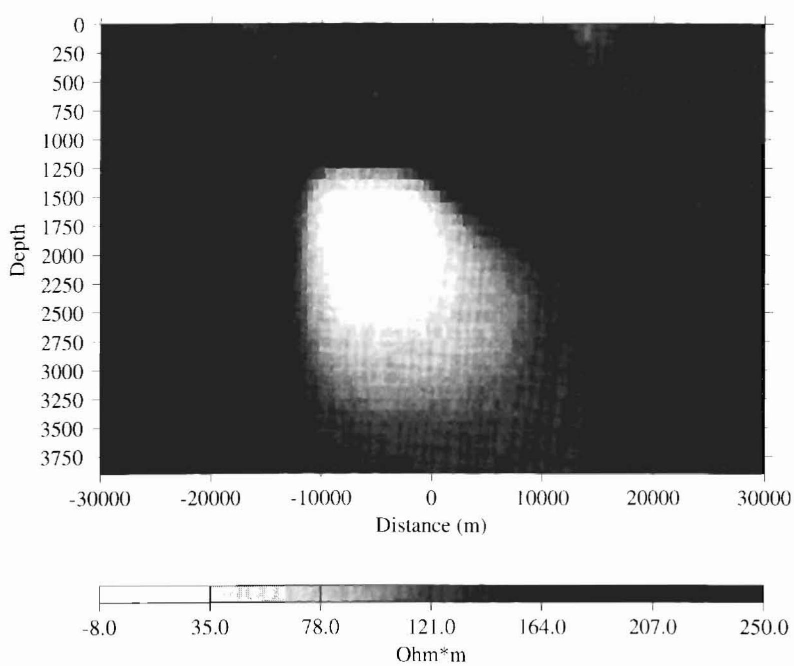

Fig. 6. The result of the 1st iteration migration imaging, stacked over the time periods range 0.01–0.25 s.

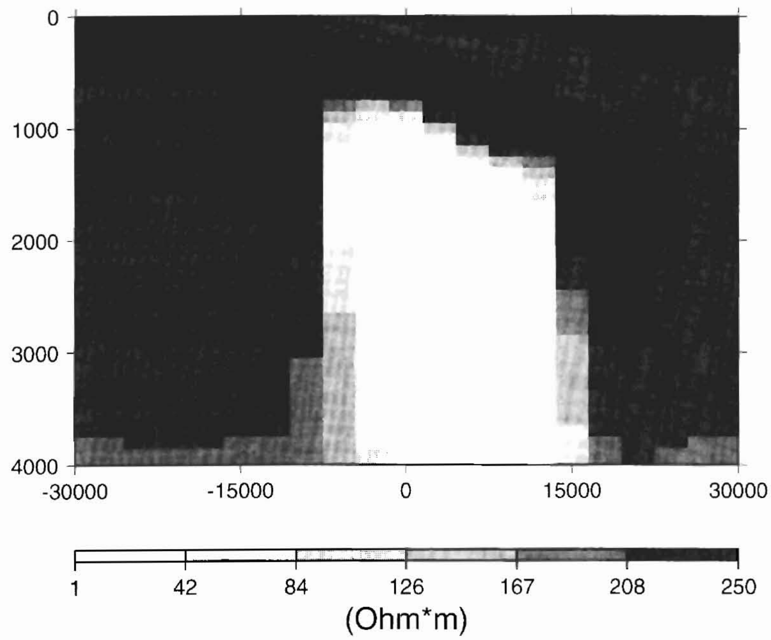

Fig. 7. The inverse model obtained for the model shown in Fig. 5 using Rapid Relaxation Inversion (RRI) code by Booker and Smith (1991) after 35 iterations.

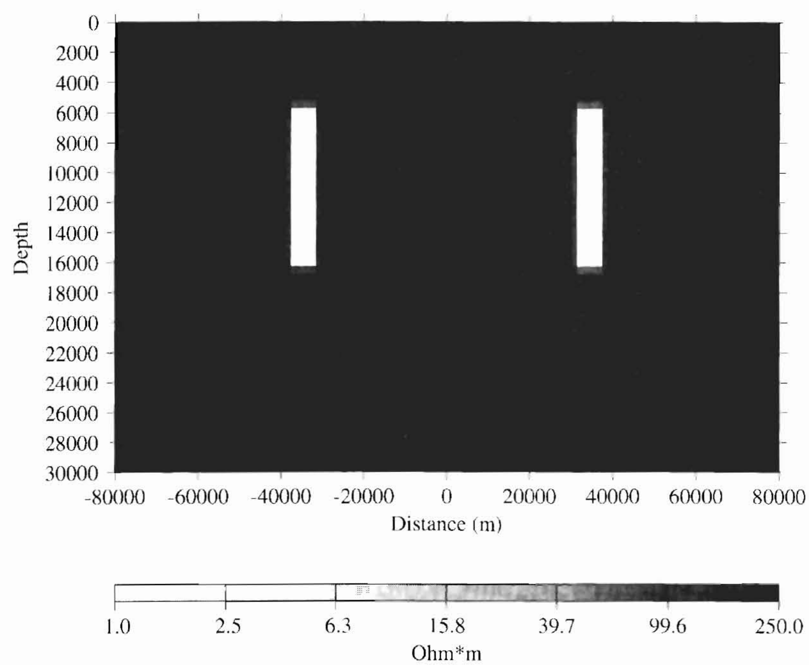

Fig. 8. 2-D resistivity model of 2 conductive rectangular inserts with resistivities 0.5 Ohm-m within a 250 Ohm-m background.

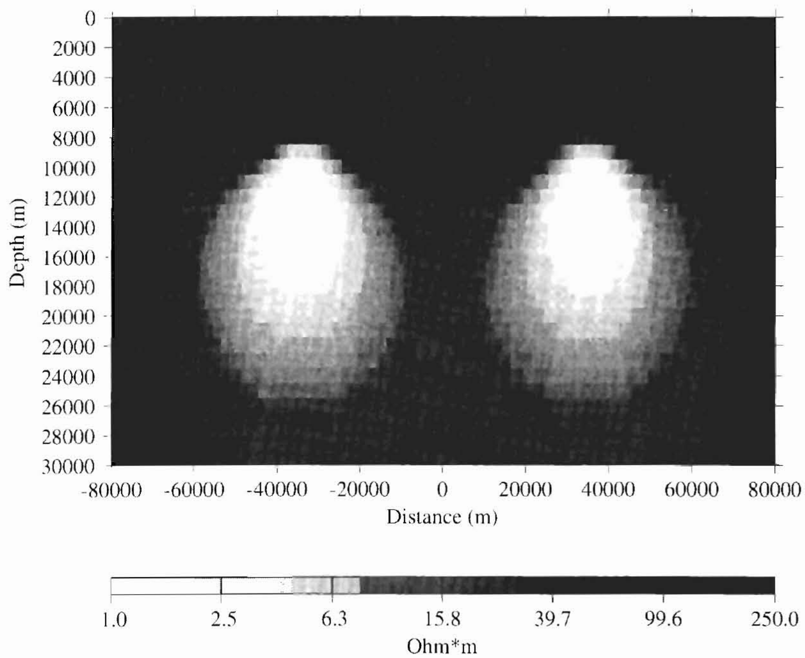

Fig. 9. The result of 1st iteration migration imaging at the time period 0.05 s for the model shown in Fig. 8.

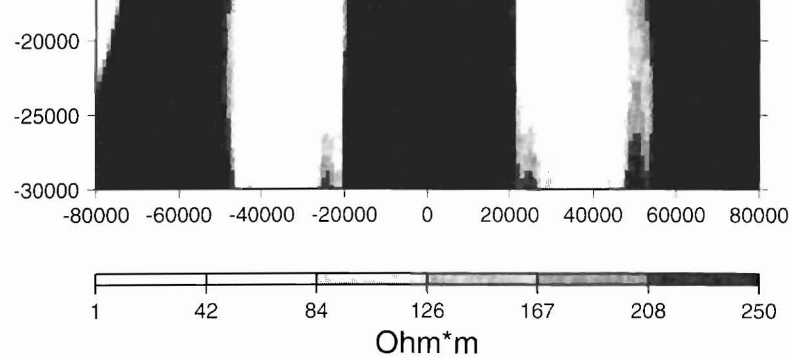

Fig. 10. The inverse model obtained for the model shown in Fig. 8 using Rapid Relaxation Inversion (RRI) code by Booker and Smith (1991) after 35 iterations.

CPU time for inversion by RRI method is 30 Min.

Imaging resistive structures is usually a more difficult task than imaging conductive objects. Figure 11 shows a model with one resistive (5000 Ohm-m) prismatic insertion, and one conductive (0.5 Ohm-m) within a 250 Ohm-m background. The synthetic "observed field" components were calculated using the same PW2D forward modeling code. The $N = 121$ observation points x_i $(i = 1, 2, \ldots, N)$ were located along the profile on the earth's surface with the separation $\Delta x = 1000$ m. We have computed the electric E_y and magnetic H_x fields for the periods 0.01–0.25 s. As we can see in Fig. 12, 1st iteration migration allows us to resolve both the resistive and the conductive objects. We have the same result even if we add 25% Gaussian noise to the observed data (Fig. 13).

So far, we have discussed results of applying migration imaging to 2-D models in TE mode. However, we can repeat for TM mode as well all the derivations made above for TE mode. We thus obtain the following imaging conditions for TM mode data:

$$\Delta\sigma_{ma}(x,z) = k_0 Re \int_{\Omega} H_y^b(x,z)\, H_y^{\Delta m}(x,z)\, d\omega. \tag{42}$$

Thus, we can see that the migration anomalous conductivity for TM mode is equal to the integral over frequencies of the product of the incident (background) magnetic field H_y^b and the migrated residual magnetic field $H_y^{\Delta m}$. Figure 14 presents the 1st iteration migration results for TM mode data, calculated for the same model shown in Fig. 11. We can see that the migration image for TM mode is exactly the same as for TE mode (Fig. 12).

We have also applied RRI method to inverse TE and TM data for the same model. The results of inversion are shown in Figs. 15 and 16. These images are compatible with those obtained

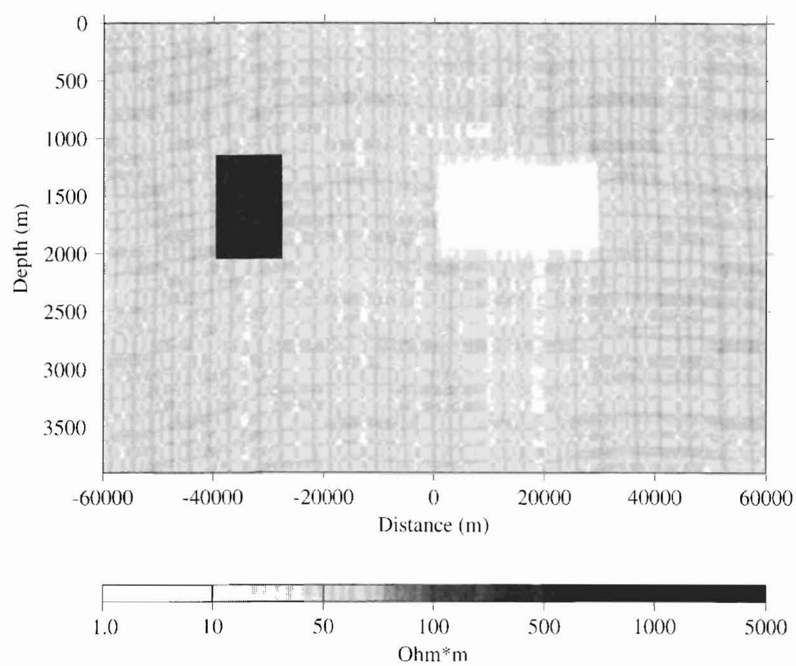

Fig. 11. 2-D resistivity model with one resistive (5000 Ohm-m) prismatic insertion, and one conductive (0.5 Ohm-m) within a 250 Ohm-m background.

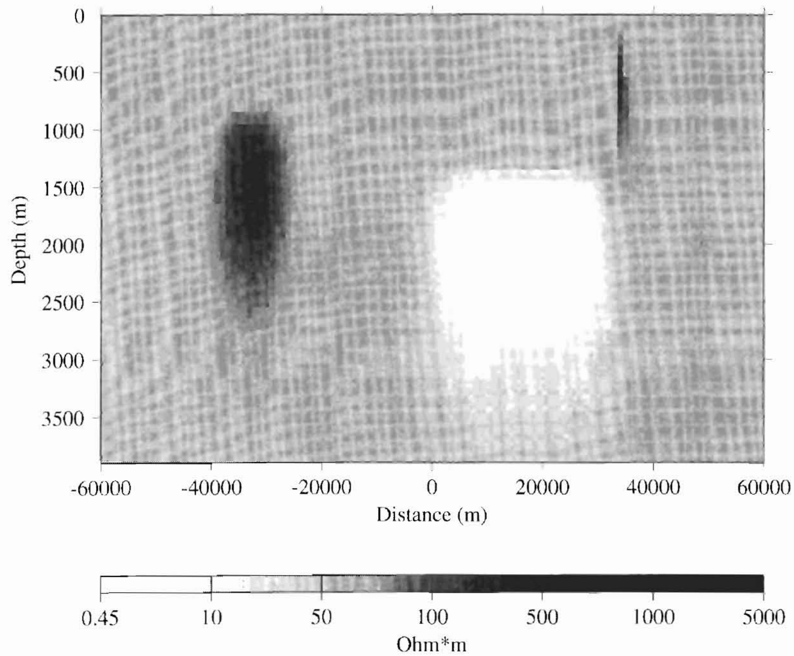

Fig. 12. The result of the 1st iteration migration imaging for TE mode, stacked over the time periods range 0.01–0.5 s for the model shown in Fig. 11.

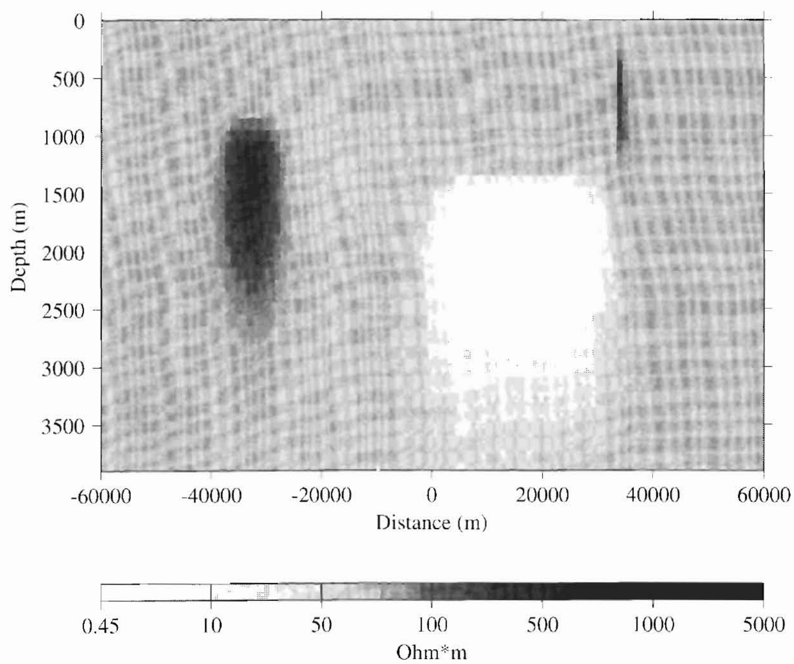

Fig. 13. The result of the 1st iteration migration imaging for TE mode, stacked over the time periods range 0.01–0.5 s for the model shown in Fig. 11 with 25% Gaussian noise added.

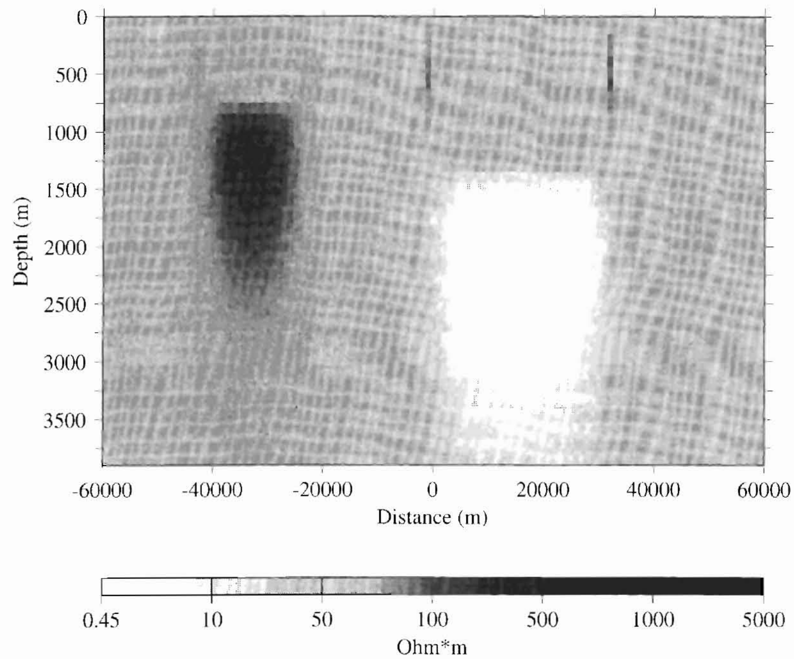

Fig. 14. The result of the 1st iteration migration imaging for TM mode, stacked over the time periods range 0.01–0.5 s for the same model shown in Fig. 11.

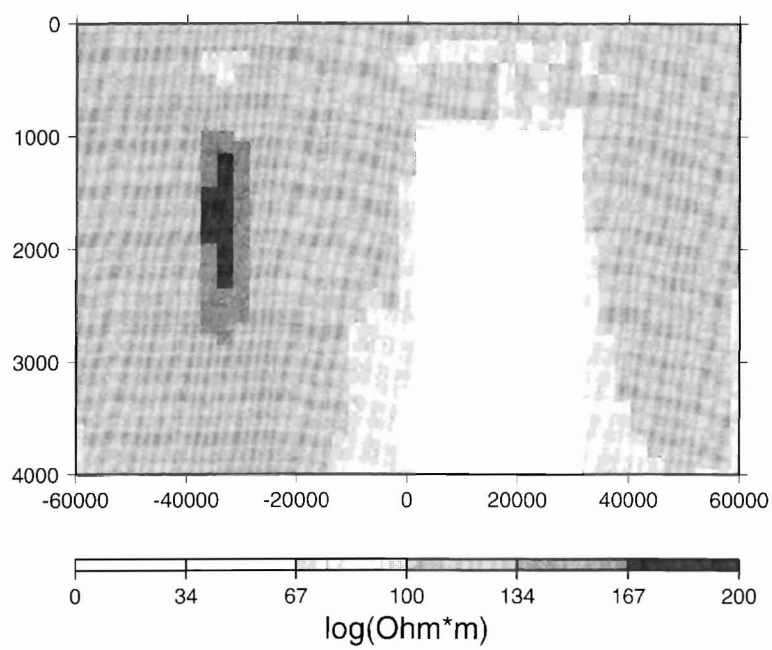

Fig. 15. The inverse model obtained for the model shown in Fig. 11 using Rapid Relaxation Inversion (RRI) code by Booker and Smith (1991) for TE mode after 35 iterations.

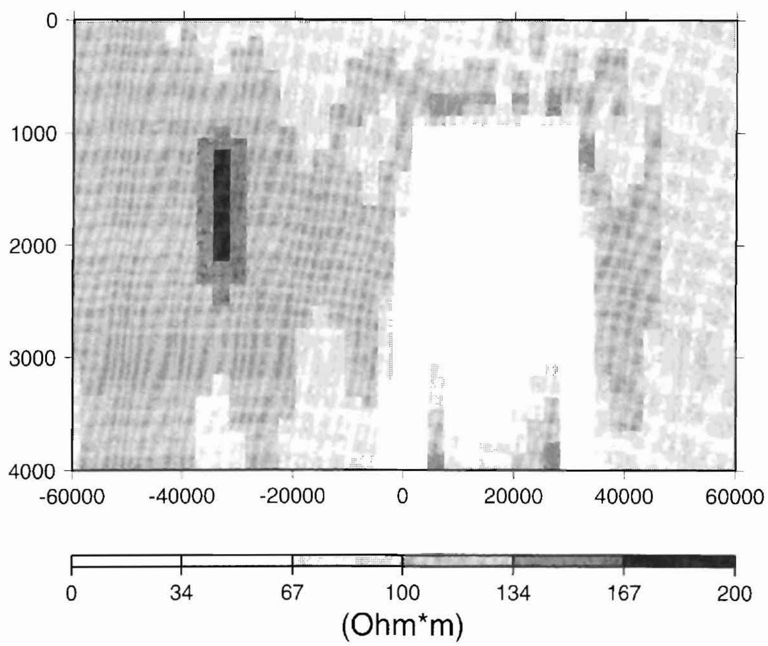

Fig. 16. The inverse model obtained for the model shown in Fig. 11 using Rapid Relaxation Inversion (RRI) code by Booker and Smith (1991) for TM mode after 35 iterations.

by migration. They produce better estimation of the depth of the resistive body. Meanwhile, the CPU time for RRI is about 35 Min for TE mode and 29 Min for TM mode, while in the case of migration it took only 23 s to actually generate the image.

6. Conclusion

The results of theoretical analysis presented in this paper demonstrate that there is a very close connection between the method of EM migration, developed in our earlier papers, and the solution of the conventional EM inverse problem. Actually, we can say now that migration is an approximate inversion. It realizes the first iteration in the inversion algorithm, based on the minimization of the residual field energy flow through the profile of observations. This new theoretical result suggests a new imaging condition formulation and indicates a new approach to EM imaging, based on iterative migration. The iterative migration forms a principally new method of interpreting EM data, which combines the ideas of downward continuation and traditional inversion. Numerical modeling demonstrates that migration generates reasonable images of the subsurface structures an order faster than rigorous inversion.

We also should notice in the conclusion that there are some limitations in using migration for interpretation of EM data. The main problem is that the background conductivity distribution used for migration should be known a priori, while in the case of conventional inversion it is usually generated in the process of inverse problem solution. Different ways of solving this problem have been discussed in our paper (Zhdanov *et al.*, 1996).

Another problem is related to the fact that the migration is based on the transformation of the electric and magnetic fields observed on the surface of the earth, and cannot handle the impedances, which are usually recorded in the case of magnetotelluric observations. Practical application of the migration would require implementation of a special observation system designed to obtain the synchronous distribution of electromagnetic field along the profiles on the earth's surface. It can be done by simultaneously using one moving observation and one fixed reference station and by applying transfer function technique to process these data. One can find more details about this technique in the book by Berdichevsky and Zhdanov (1984).

Financial support for this work was provided by the National Science Foundation under grant No. EAR-9403925.

We also thank the University of Utah Consortium of Electromagnetic Modeling and Inversion (CEMI), which includes CRA Exploration Ltd., Mindeco, MIM Exploration, Naval Research Laboratory, Newmont Exploration, Western Mining, Kennecott Exploration, Schlumberger-Doll Research, Shell International Exploration and Production, Western Atlas, Western Mining, the United States Geological Survey, Unocal Geothermal Corporation, and Zonge Engineering for providing additional support for this work.

We are thankful to the reviewers, Drs. C. Farquharson and D. Avdeev, for their helpful remarks.

Appendix A: Calculation of the First Variation of Electromagnetic Field

Perturbing Eq. (1) we obtain the equation for the first variation of the electric field:

$$\nabla^2 \delta E_y + i\omega\mu_0\sigma\delta E_y = \begin{cases} -i\omega\mu_0\delta\sigma E_y, & (x,z) \in D \\ 0, & (x,z) \notin D \end{cases}. \tag{A.1}$$

We now introduce the Green's function G_σ of the geoelectrical model with the conductivity $\sigma = \sigma(x,z)$. The Green's function depends on the position of the points (x,z) and (x',z') and is determined by the equation:

$$\nabla^2 G_\sigma(x,z\,|x',z') + i\omega\mu_0\sigma G_\sigma(x,z\,|x',z') = -\delta(x-x',z-z'), \tag{A.2}$$

where $\delta(x-x',z-z')$ is two-dimensional Dirac function.

According to the Green's formula:

$$\int_L \left(\frac{\partial \delta E_y}{\partial \mathbf{n}} G_\sigma - \frac{\partial G_\sigma}{\partial \mathbf{n}} \delta E_y\right) dl = \iint_S \left(G_\sigma \nabla^2 \delta E_y - \delta E_y \nabla^2 G_\sigma\right) ds, \tag{A.3}$$

where $\mathbf{n}$ is the direction of the outer normal to L.

Let us assume now that the region S is a big circle with the center inside domain D and of radius R which is so big that $D \subset S$. Taking into account Eqs. (A.1) and (A.2) the Eq. (A.3) can be rewritten as:

$$\int_L \left(\frac{\partial \delta E_y}{\partial \mathbf{n}} G_\sigma - \frac{\partial G_\sigma}{\partial \mathbf{n}} \delta E_y\right) dl = \iint_S \left(-i\omega\mu_0 G_\sigma \delta\sigma E_y + \delta E_y \delta(x-x',z-z')\right) ds. \tag{A.4}$$

Let us expand the radius R of the circle L to infinity. Then the curvilinear integral will go to zero, because, due to the radiation conditions, functions δE_y and G_σ vanish rapidly at infinity, and we finally obtain:

$$\delta E_y(x',z') = i\omega\mu_0 \iint_D G_\sigma(x-x',z-z') \cdot \delta\sigma(x,z)\, E_y(x,z)\, ds. \tag{A.5}$$

The first variation of the magnetic field δH_x can be calculated from δE_y using Maxwell's equations:

$$\delta H_x(x',z') = -\frac{1}{i\omega\mu_0}\frac{\partial \delta E_y(x',z')}{\partial z'} = -\iint_D \frac{\partial G_\sigma(x-x',z-z')}{\partial z'} \delta\sigma(x,z)\, E_y(x,z)\, ds, \tag{A.6}$$

where domain of integration changes from S to D because of Eq. (14).

Appendix B: Integral Representations for Electromagnetic Migration Field

Following our previous publications (Zhdanov and Keller, 1994; Zhdanov *et al.*, 1996), we introduce the EM migration field as the solution of the boundary value problem for the adjoint Maxwell's equation. In the case of E-polarization and in the frequency domain, the E_y^{m*} component of the EM migration field satisfies the equation:

$$\nabla^2 E_y^{m*} - i\omega\mu_0\sigma E_y^{m*} = 0, \ z \geq 0 \tag{B.1}$$

everywhere in the lower half-plane, vanishes according to the radiation conditions at the infinity, and is equal to the observed field on the surface of observation $z' = 0$:

$$E_y^{m*}(x', z=0, \omega) = E_y(x', z=0, \omega),$$
$$\left.\frac{\partial E_y^{m*}(x', z', \omega)}{\partial z'}\right|_{z'=0} = \left.\frac{\partial E_y(x', z', \omega)}{\partial z'}\right|_{z'=0}, \tag{B.2}$$

where asterisk $*$ denotes complex conjugate values.

We have the same conditions for the migrated residual field E_y^{Δ}:

$$\nabla^2 E_y^{\Delta m*} - i\omega\mu_0\sigma E_y^{\Delta m*} = 0, \ z \geq 0 \tag{B.3}$$

and

$$E_y^{\Delta m*}(x', o, \omega) = E_y^{\Delta}(x', o, \omega)$$

$$\left.\frac{\partial E_y^{\Delta m*}(x', z', \omega)}{\partial z'}\right|_{z'=0} = \left.\frac{\partial E_y^{\Delta}(x', z', \omega)}{\partial z'}\right|_{z'=0}$$

The complex conjugated Green's function $G_{\sigma_b}^*$ satisfies the following equation in the lower half-plane:

$$\nabla^2 G_{\sigma_b}^*(x, z\,|x', z') - i\omega\mu_0\sigma G_{\sigma_b}^*(x, z\,|x', z') = -\delta(x - x', z - z'). \tag{B.4}$$

We can now apply Green's formula taking into account Eqs. (B.3) and (B.4) and repeating the derivations similar to the one described in Appendix A. As the result, we find the expression for the migrated residual electric field as an integral over the profile of observations, horizontal axis x, of the residual electric field:

$$\int_{-\infty}^{+\infty}\left(G_{\sigma_b}^*(x, z\,|x', z')\frac{\partial E_y^{\Delta}(x', z')}{\partial z'} - E_y^{\Delta}(x', z')\frac{\partial G_{\sigma_b}^*(x, z\,|x', z')}{\partial z'}\right)_{z'=0} dx'$$
$$= E_y^{\Delta m*}(x, z). \tag{B.5}$$

Taking complex conjugated values of the left-hand and right-hand parts of Eq. (B.5) we determine:

$$\int_{-\infty}^{+\infty}\left(G_{\sigma_b}(x, z\,|x', z')\frac{\partial E_y^{\Delta *}(x', z')}{\partial z'} - E_y^{\Delta *}(x', z')\frac{\partial G_{\sigma_b}(x, z\,|x', z')}{\partial z'}\right) dx'$$
$$= E_y^{\Delta m}(x, z). \tag{B.6}$$

The last two equations give the integral representations for the solution of the boundary value problem for the migrated residual field.

Appendix C: Definition of the Length of the Step k_0

The optimal length of the step k_0 can be determined by minimization of the functional $\Phi\left[\sigma_b(x,z) - k_0 l(x,z)\right] = \Phi(k_0)$.

We denote by $E_y^{(1)}$, $H_x^{(1)}$ the EM field components corresponding to the geoelectrical model with the conductivity distribution $\sigma = \sigma_b(x,z) - k_0 l(x,z)$. Let us substitute $E_y^{(1)}$, $H_x^{(1)}$ into Eq. (12),

$$\Phi = \frac{1}{4}\int_{\Omega}\int_{-\infty}^{+\infty}\left(E_y^{(1)\Delta}H_x^{(1)\Delta *} + E_y^{(1)\Delta *}H_x^{(1)\Delta}\right)dx'd\omega, \tag{C.1}$$

where $E_y^{(1)\Delta} = E_y^{obs} - E_y^{(1)}$, $H_x^{(1)\Delta} = H_x^{obs} - H_x^{(1)}$, and the calculation of theoretical field $E_y^{(1)}$, $H_x^{(1)}$ is linearized, using Born approximation (Berdichevsky and Zhdanov, 1984):

$$\begin{aligned} E_y^{(1)} &= E_y^{(1)}(x',o,\omega) \approx E_y^b(x',o,\omega) + i\omega\mu_0\iint_S G_{\sigma_b}(x-x',z)\,\delta\sigma(x,z)\,E_y^b(x,z)\,ds \\ &= E_y^b(x',o,\omega) - k_0E_y^l(x',o,\omega), \end{aligned} \tag{C.2}$$

$$\begin{aligned} H_x^{(1)} &= H_x^{(1)}(x',o,\omega) \approx H_x^b(x',o,\omega) - \iint_S \frac{\partial G_{\sigma_b}(x-x',z-z')}{\partial z'}\Big|_{z'=0}\,\delta\sigma(x,z)\,E_y^b(x,z)\,ds \\ &= H_x^b(x',o,\omega) - k_0H_x^l(x',o,\omega), \end{aligned} \tag{C.3}$$

where $\delta\sigma(x,z) = -k_0 l(x,z)$ and E_y^l, H_x^l are the fields, calculated using Born approximation for the model, perturbed in the gradient direction:

$$E_y^l(x',o,\omega) = i\omega\mu_0\iint_S G_{\sigma_b}(x-x',z)\,l(x,z)\,E_y^b(x,z)\,ds, \tag{C.4}$$

$$H_x^l = -\frac{1}{i\omega\mu_0}\frac{\partial E_y^l}{\partial z'}. \tag{C.5}$$

Substituting Eqs. (C.2) and (C.3) into Eq. (C.1), we obtain:

$$\begin{aligned} \Phi &= \frac{1}{4}\int_{\Omega}\int_{-\infty}^{+\infty}\left(E_y^{(1)\Delta}H_x^{(1)\Delta *} + E_y^{(1)\Delta *}H_x^{(1)\Delta}\right)dx'd\omega \\ &= \frac{1}{4}\int_{\Omega}\int_{-\infty}^{+\infty}\Big\{\left[E_y^{\Delta} + k_0E_y^l\right]\left[H_x^{\Delta} + k_0H_x^l\right]^* \\ &\qquad + \left[E_y^{\Delta} + k_0E_y^l\right]^*\left[H_x^{\Delta} + k_0H_x^l\right]\Big\}\,dx'd\omega. \end{aligned} \tag{C.6}$$

Now we can find the first variation of $\Phi(k_0)$ with respect to k_0:

$$\begin{aligned} \delta_{k0}\Phi(k_0) = \frac{1}{4}\delta k_0\int_{\Omega}\int_{-\infty}^{+\infty}&\left\{\left[E_y^lH_x^{\Delta *} + E_y^{\Delta}H_x^{l*} + E_y^{l*}H_x^{\Delta} + E_y^{\Delta *}H_x^l\right]\right. \\ &\left. + 2k_0\left[E_y^lH_x^{l*} + E_y^{l*}H_x^l\right]\right\}dx'd\omega. \end{aligned} \tag{C.7}$$

After some algebraic transformations, we obtain:

$$\delta_{k0}\Phi(k_0) = \frac{1}{2}\delta k_0\int_{\Omega}\int_{-\infty}^{+\infty}\left\{Re\left[E_y^lH_x^{\Delta *} + E_y^{\Delta}H_x^{l*}\right] + 2k_0Re\left[E_y^lH_x^{l*}\right]\right\}dx'd\omega. \tag{C.8}$$

The necessary condition for minimizing $\Phi(k_0)$ is:

$$\delta_{k_0}\Phi(k_0) = 0.$$

Therefore, we have:

$$\int_{\Omega}\int_{-\infty}^{+\infty}\left\{Re\left[E_y^l H_x^{\Delta *} + E_y^{\Delta} H_x^{l*}\right] + 2k_0 Re\left[E_y^l H_x^{l*}\right]\right\} dx' d\omega = 0.$$

From the last equation we find at once:

$$k_0 = -\frac{Re\int_{\Omega}\int_{-\infty}^{+\infty}\left[E_y^l H_x^{\Delta *} + E_y^{\Delta} H_x^{l*}\right] dx' d\omega}{2Re\int_{\Omega}\int_{-\infty}^{+\infty} E_y^l H_x^{l*} dx' d\omega}. \tag{C.9}$$

REFERENCES

Berdichevsky, M. N. and M. S. Zhdanov, *Advanced Theory of Deep Geomagnetic Sounding*, 408 pp., Elsevier, Amsterdam, 1984.

Pankratov, O. V., D. B. Avdeev, and A. V. Kuvshinov, Scattering of electromagnetic field in inhomogeneous earth. Forward problem solution, *Fizika Zemli*, No. 3, 17–25, 1995.

Smith, J. T. and J. R. Booker, Rapid inversion of two- and three-dimensional magnetotelluric data, *J. Geophys. Res.*, **96**, 3905–3922, 1991.

Stratton, J. A., *Electromagnetic Theory*, 615 pp., McGraw-Hill Book Company, New-York and London, 1941.

Tarantola, A., *Inverse Problem Theory*, 613 pp., Springer-Verlag, Berlin, Heidelberg, New York, 1987.

Wannamaker, P. E., J. A. Stodt, and L. Rijo, A stable finite element solution for two-dimensional magnetotelluric modeling, *Geoph. J. Roy. Astr. Soc.*, **88**, 277–296, 1987.

Zhdanov, M. S., Tutorial: Regularization in inversion theory, Colorado School of Mines, 1993.

Zhdanov, M. S. and G. V. Keller, *The Electromagnetic Methods in Geophysical Exploration*, 873 pp., Elsevier, Amsterdam, 1994.

Zhdanov, M. S. and O. Portniaguine, Time domain electromagnetic migration in the solution of the inverse problems, *Geophys. J. Int.*, 1997 (in press).

Zhdanov, M. S., P. Traynin, and O. Portniaguine, Resistivity imaging by time domain electromagnetic migration, *Explor. Geophys.*, **26**, 186–194, 1995.

Zhdanov, M. S., P. Traynin, and J. Booker, Underground imaging by frequency domain electromagnetic migration, *Geophysics*, **61**, 3, 1996.